

Theory of energy deposition by suprathermal electrons in laser-irradiated targets

David Salzmann*

*Institute of Laser Engineering, Osaka University, 2-6 Yamada-oka, Suita, Osaka 565-8071, Japan
and Soreq NRC, Yavne 81800, Israel*

(Received 25 October 2001; published 17 May 2002)

In this paper we describe results of the preheat generated by the suprathermal electrons from laser-produced plasmas in the cold substrate material. The computations were carried out by means of a Monte Carlo-type code that accounts for the scattering and slow down of the hot electrons in the cold material. Using ideas derived from a straight-line approximation method, the results were described by means of a dimensionless quantity. Such a description results in simple analytical (in fact, exponential) formulas, which are easy for computation and can be readily inserted into hydrodynamics codes. To exemplify the results, we have computed the preheat temperature and pressure in a laser-irradiated aluminum foil. A short discussion is given about the accuracy and the validity domain of the formulas, and a comparison is given to previous analytical methods.

DOI: 10.1103/PhysRevE.65.056409

PACS number(s): 52.38.-r, 52.20.Fs, 52.25.Tx

I. INTRODUCTION

Target preheat by suprathermal electrons generated near the critical density surface plays an important role in several aspects of laser-produced plasmas. These very fast electrons run into the cold substrate ahead of the ablation shock wave, preheating the target material, thereby generating a backward pressure.

The role of the suprathermal electrons (called also “hot” or “fast” electrons) in laser-produced plasmas was extensively studied by experimental means [1–8]. The theoretical backup for these studies is, however, relatively scarce. In fact, to the best of our knowledge, only the pioneering article of Harrach and Kidder [9] tries to give some analytical formulas that can provide a partial view on the behavior of this phenomenon as a function of various physical parameters. Since their publication, however, there had been great progress in this field both in the understanding of this phenomenon, as well as in the computational capabilities and the accuracy of the underlying databases. It seems that the time has come for an update of the whole subject in view of the knowledge accumulated since their paper.

A brief list of the hot electron properties is in order. The electron energy distribution in laser-produced plasmas consists of two parts: most of the electrons are part of a Maxwell-Boltzmann velocity distribution characterized by the plasma temperature T . This energy distribution has, however, a high energy “tail” that has an exponentially decreasing shape. This exponential tail is the definition of the suprathermal electrons,

$$n_{e,\text{hot}}(E_0)dE_0 = N_h \frac{1}{T_h} \exp\{-E_0/T_h\} dE_0 \quad (1)$$

(in the following we use units in which temperatures are measured in energy units, i.e., the Boltzmann constant $k = 1$), N_h is the total number of the suprathermal electrons and T_h is the hot temperature. The suprathermal electrons are

generated near the critical surface, and their initial motion is strongly forward directed. They move rapidly through the hot plasma layer behind the critical surface, and penetrate into the cold substrate material. The effect of these fast electrons on the cold matter can be regarded as that of a flux of electrons, with energy distribution described by Eq. (1), hitting the surface of a cold material. This surface, that divides between the hot plasma and the cold material is taken in the following as $x=0$, see Fig. 1.

A compilation of experiments at which the hot temperature had been measured indicates [10] that this quantity follows a power law behavior as a function of the quantity $I_L \lambda^2$ (I_L is the laser intensity in W/cm^2 and λ is the laser wavelength),

$$T_h = T_0 \left(\frac{I_L \lambda^2}{(I_L \lambda^2)_0} \right)^\beta. \quad (2)$$

In Eq. (2) $(I_L \lambda^2)_0$ is a reference point, T_0 is the value of the hot temperature for $I_L \lambda^2 = (I_L \lambda^2)_0$, and β is a constant whose value is close to $1/3$ [10]. Numerically Eq. (2) can be rewritten as

$$T_h = (7 \text{ keV}) \times I_{15}^{1/3},$$

$$\text{where } I_{15} = I_L \lambda^2 / (10^{15} \text{ W } \mu\text{m}^2/\text{cm}^2). \quad (3)$$

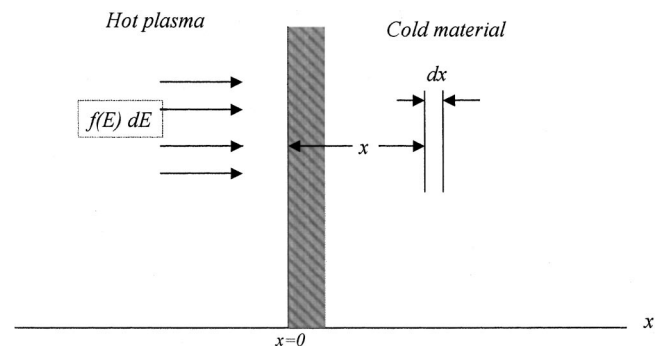


FIG. 1. Description of the basic geometry of suprathermal electron preheat.

*On sabbatical leave from Soreq NRC, Yavne 81800, Israel.

All the hot temperatures in experiments with laser-produced plasmas, up to $I_L \lambda^2 \leq 3 \times 10^{17} \text{ W } \mu\text{m}^2/\text{cm}^2$, are distributed around Eq. (3), although the fluctuations are large. At higher intensities, when the hot electrons become relativistic, the exponent β changes to a higher value, close to 1. Our computations are not valid at such high intensities, see below.

The total energy of the hot electrons $N_h T_h$ is connected to the total laser energy E_L by

$$N_h T_h = \eta E_L. \quad (4)$$

η is the fraction of laser energy channeled into suprathermal electron production. η depends on various experimental factors, such as the pulse shape, prepulse, etc. It is, however, at a level of a few percent in most experiments, sometimes up to $\eta \sim 10\%$ or more.

The aim of the present paper is to calculate the energy deposition, as function of depth, in a cold substrate material hit by a flux of hot electrons. We do this calculation in two steps.

First we use the straight line approximation (SLA), assuming that the fast electrons move along straight trajectories (Sec. II). The purpose of this relatively crude approximation is to obtain analytical albeit low accuracy results, which can nevertheless provide an insight into the central parameters of the problem.

Second, full Monte Carlo simulations were carried out for several target materials and hot electron energy temperatures (Sec. III). To get the best accuracy, in these simulations we have used updated databases for the electron cross sections and stopping power. The results of the simulations were parametrized into semiempirical formulas by using the ideas derived from the SLA method. The simple form of these final semiempirical formulas enable their direct application in hydrodynamics codes. For purposes of illustration, we show in Sec. III D the preheat temperature and pressure generated by the suprathermal electrons in an aluminum target irradiated by a 10^{15} W/cm^2 intense laser beam.

Finally in Sec. IV we present a short discussion of the validity domain of the computations, the accuracy of the results, and a comparison to the results of Ref. [9].

II. THE SUPRATHERMAL ELECTRON PREHEAT IN THE SLA

The SLA model considers a flux of hot electrons hitting a homogeneous cold solid target of density n_A (atoms per unit volume). Our starting point is the notion that for electron energies between 1 and 100 keV, the stopping power $|\partial E/\partial x|$ in any material follows very closely a power law decrease [9,11] (in the following our basic units are cm, eV, s):

$$\left| \frac{\partial E}{\partial x} \right| = B E^{-\alpha}, \quad [B] = \frac{\text{eV}^{1+\alpha}}{\text{cm}}, \quad (5)$$

where B and α are constants specific to the target material. Equation (5) is a well-known parametrization [9] of the tables of the stopping power [11] in the given range. In general, the parameter α is a positive number smaller than 1,

with values between $\alpha \approx 0.75$ (aluminum) and $\alpha \approx 0.66$ (gold) (these numbers are the result of parametrization of the numerical tables of [11]). B also has a rather limited variation, between 3.95×10^{10} for aluminum up to 7.47×10^{10} for gold. Above 100 keV the stopping power shows significant deviation from this simple form, mainly due to relativistic effects.

The basic approximation of SLA is that the electrons move along straight lines. Under this approximation, the relationship between the initial energy of an electron on the target surface E_0 and its energy $E(x)$ at depth x is given by

$$\begin{aligned} x &= \int_0^x dx = \int_E^{E_0} \frac{dE}{|\partial E/\partial x|} = \int_E^{E_0} \frac{dE}{B E^{-\alpha}} \\ &= \frac{1}{B} \int_E^{E_0} E^\alpha dE = \frac{1}{(1+\alpha)B} (E_0^{1+\alpha} - E^{1+\alpha}), \end{aligned} \quad (6)$$

$$E(x) = [E_0^{1+\alpha} - (1+\alpha)Bx]^{1/(1+\alpha)}. \quad (7)$$

It follows that the energy, $\delta E(E_0, x)$, deposited by an electron of initial energy E_0 along the path $[x, x + \delta x]$ at depth x inside the target is given by

$$\begin{aligned} \delta E(E_0, x) &= \delta x \left| \frac{\partial E}{\partial x} \right| \\ &= \delta x B E^{-\alpha} \\ &= \delta x B [E_0^{1+\alpha} - (1+\alpha)Bx]^{-\alpha/(1+\alpha)}. \end{aligned} \quad (8)$$

The *energy deposition per atom* is obtained by replacing δx in Eq. (8) by the interatomic distance $D = n_A^{-1/3}$. The basic picture underlying Eq. (8) is of one single electron moving along an array of atoms, losing energy gradually during its motion. To get the energy deposition by the whole hot electron distribution, one has to multiply the above equation by the number of hot electrons that hit every array of atoms, and, of course, by the electron energy distribution. The hot electron areal density is N_h/S_L where S_L is the laser beam focal area, whereas the number of atoms per unit area on the target surface is $n_A D$. The ratio of these two densities is equal to the number of hot electrons per array of atoms. The total energy deposition per atom at depth x is, therefore,

$$\begin{aligned} \Delta E(x) &= \frac{N_h/S_L}{n_A D} \int dE_0 \frac{n_{e,\text{hot}}(E_0)}{N_h} \\ &\quad \times DB [E_0^{1+\alpha} - (1+\alpha)Bx]^{-\alpha/(1+\alpha)} \\ &= \frac{N_h}{n_A S_L} \frac{B}{T_h} \int dE_0 e^{-E_0/T_h} \\ &\quad \times [E_0^{1+\alpha} - (1+\alpha)Bx]^{-\alpha/(1+\alpha)}. \end{aligned} \quad (9)$$

The integration is carried out only for the E_0 's for which the first term in the square brackets is larger than the second one, or in other words, only for those electrons whose initial energy E_0 provides a range larger than x . We define the dimensionless parameter y_0 by

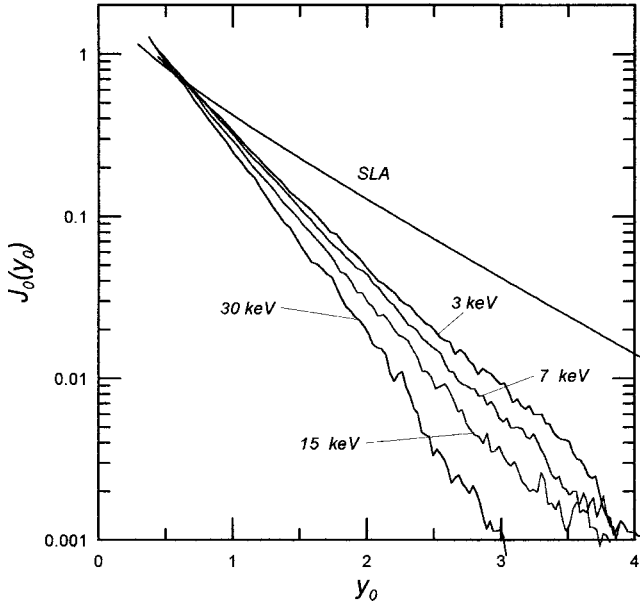


FIG. 2. The behavior of the function $J_0(y_0)$ as a function of y_0 , for an aluminum target in the SLA model, and the Monte Carlo simulations results for hot temperatures of 3, 7, 15, and 30 keV.

$$y_0(x) = \frac{[(1 + \alpha)Bx]^{1/(1+\alpha)}}{T_h} \quad (10)$$

and change the variable of the integration to $y = E_0/T_h$. Then Eq. (9) is reduced to

$$\Delta E(x) = \frac{N_h}{n_A S_L} B T_h^{-\alpha} \int_{y_0}^{\infty} dy e^{-y} [y^{1+\alpha} - y_0^{1+\alpha}]^{-\alpha/(1+\alpha)}. \quad (11)$$

It should be noted that this expression depends on the depth inside the target x , only through the variable $y_0(x)$, and on the target material through B and α . Denote the dimensionless integral in Eq. (11) by

$$J_0(y_0) = \int_{y_0}^{\infty} dy e^{-y} [y^{1+\alpha} - y_0^{1+\alpha}]^{-\alpha/(1+\alpha)}, \quad (12)$$

then

$$\Delta E(x) = \frac{N_h}{n_A S_L} B T_h^{-\alpha} J_0(y_0) \frac{\text{eV}}{\text{atom}}. \quad (13)$$

Equation (13) gives the energy deposition per atom at depth x . The total energy deposited by all the hot electrons at all depths is, of course, the hot electrons total energy,

$$\Delta E_{\text{tot}} = \int_0^{\infty} \Delta E(x) dx = N_h T_h. \quad (14)$$

Indeed, integrating both sides of Eq. (13) over x one can reproduce Eq. (14) rigorously. The interesting physics of our problem is contained in the function $J_0(y_0)$. In Fig. 2 we

show this function for an aluminum target hit by a flux of hot electrons of $T_h = 7$ keV. Figure 2 indicates that an exponential function of the form

$$J_0(y_0) \cong A \exp\{-ay_0\} \quad (15)$$

provides an excellent approximation to this function. Similar behavior was found for all the materials in our study. In view of Eq. (14) A and a have to satisfy a relationship,

$$A = a^{1+\alpha}/\Gamma(1+\alpha). \quad (16)$$

The values derived from Fig. 2 are $A = 1.35$ and $a = 1.17$. These values satisfy Eq. (16) to within 6%, and this small difference can be regarded as a measure of the deviation of $J_0(y_0)$ from an accurate exponential behavior.

Using Eqs. (1)–(4), Eq. (13) can be rewritten in terms of the laser-irradiation parameters as follows:

$$\begin{aligned} \Delta E(x) &= \frac{\eta E_L}{n_A S_L T_h} B T_h^{-\alpha} J_0(y_0) \\ &= \frac{\eta I_L \tau_L}{n_A} B T_h^{-(1+\alpha)} J_0\left(\frac{[(1+\alpha)Bx]^{1/(1+\alpha)}}{T_h}\right). \end{aligned} \quad (17)$$

In Eq. (17) τ_L is the laser pulse duration. Denote by $Q = B \times (7 \text{ keV})^{-\alpha} = |\partial E/\partial x|_{E=7 \text{ keV}}$ the stopping power of the substrate material for electrons of 7 keV, see Eq. (3), and by $\tau_{L,\text{ps}} = \tau_L/10^{-12}$ s, the laser pulse duration in ps. Using these notations, Eq. (17) can be cast into a useful numerical form,

$$\begin{aligned} \Delta E(x) &= (8.92 \times 10^{17} \text{ cm}^{-2}) \times \frac{\eta Q}{n_A} \tau_{L,\text{ps}} I_{15}^{(2-\alpha)/3} \\ &\quad \times J_0\{I_{15}^{-1/3} [(1.43 \times 10^{-4} \text{ eV}^{-1}) \\ &\quad \times (1+\alpha) Q x]^{1/(1+\alpha)}\}, \end{aligned} \quad (18)$$

Equations (17) and (18) are the final results of the SLA method. An example can help in illustrating these results. For aluminum, the values of the parameters of the stopping power are $\alpha = 0.7369$, $B = 3.95 \times 10^{10} \text{ eV}^{1.7369}/\text{cm}$, resulting in $Q = 5.80 \times 10^7 \text{ eV}/\text{cm}$. Inserting the above values for A and a into Eq. (18) one gets the SLA result for aluminum ($x_{\mu\text{m}}$ is the depth in μm),

$$\begin{aligned} \Delta E(x) &= (1160 \text{ eV}) \times \eta \tau_{L,\text{ps}} I_{15}^{0.4210} \\ &\quad \times \exp\{-1.46 x_{\mu\text{m}}^{0.5757} I_{15}^{-1/3}\}. \end{aligned} \quad (19)$$

III. RESULTS OF THE MONTE CARLO SIMULATIONS

A. Description of the Monte Carlo code

The drawbacks of the SLA method are connected to its inability to account for the scattering of the suprathermal electrons inside the target. Scattering reduces the hot electron penetration depth, and even backscatters a significant fraction of energy into the hot plasma, thereby reducing the energy deposited inside the cold material. To account for these

TABLE I. The properties of the target materials used in the computations and the results of the Monte Carlo simulations for the absorbed and backreflected energy, as well as the parameters of the exponential fit to the energy deposition per atom. The numbers in brackets denote the power of 10.

	Aluminum	Titanium	Copper	Erbium	Gold	
Z	13	22	29	68	79	
ρ (g/cm ³)	2.699	4.54	8.96	9.066	19.32	
B	3.95 [10]	5.21 [10]	7.78 [10]	7.35 [10]	7.47 [10]	
α	0.7369	0.7242	0.7057	0.7650	0.6593	
Q (eV/cm)	5.80 [7]	8.55 [7]	15.05 [7]	18.66 [7]	21.79 [7]	
Absorbed energy (%)	3 keV	82.4	79.3	80.5	77.4	69.7
	7 keV	78.6	72.7	74.9	70.3	66.2
	15 keV	74.0	67.3	67.8	62.5	59.5
	30 keV	69.1	61.5	62.1	55.1	52.5
Backreflected energy (%)	3 keV	17.6	20.7	19.2	22.8	31.3
	7 keV	21.4	26.3	25.1	29.7	33.8
	15 keV	26.0	32.7	32.3	37.5	40.6
	30 keV	30.9	38.5	37.9	44.9	47.5
A	3 keV	2.12	2.46	2.36	2.33	2.22
	7 keV	2.70	3.05	3.00	3.32	3.23
	15 keV	2.90	3.34	3.38	3.84	3.80
	30 keV	3.20	4.08	3.81	4.79	4.78
a	3 keV	1.86	2.07	2.00	2.14	2.23
	7 keV	2.13	2.37	2.31	2.59	2.70
	15 keV	2.29	2.62	2.62	3.02	3.11
	30 keV	2.52	3.11	2.99	3.73	3.94

effects, we developed a Monte Carlo (MC) type code to simulate the motion of the electrons inside the cold substrate.

The code is based on the continuous slowing down approximation (CSDA) [12]. In this method the electrons change their direction of motion due to elastic scattering, and between two scattering points they lose energy continuously. The database for the simulations, namely the elastic scattering cross section and the stopping power, were taken from Ref. [11], which to the best of our knowledge have the highest available accuracy to date. The angular distribution of the elastic scattering was parametrized from the tables of Ref. [13].

The accuracy of the code was checked by simulating previous experiments in which electron transmission through thin foils were measured [14,15]. The code could reproduce the results of all these experiments to better than the experimental inaccuracies.

Computations were carried out for hot temperatures between 3–30 keV and for targets of aluminum, titanium, copper, erbium, and gold, thereby covering a range of targets from low to high atomic numbers. We were interested mainly in two parameters, the percentage of the absorbed/backreflected energies, and the energy deposition as function of the depth inside the cold target.

B. The absorbed and the backreflected energy

The electrons change direction in the target due to the elastic scattering. For some electrons the change can be large enough, so that after several scatterings they move backward relative to their initial direction, and are even backscattered

into the hot part of the plasma. The percentage of the energy absorbed in the cold substrate material, as well as the percentage of the energy backscattered into the hot plasma, are shown in Table I for the materials and the hot temperatures used in the simulations. It can be seen that there is a general tendency, so that less energy is backreflected (and, therefore more is absorbed) for lower hot temperatures than for higher ones, and less is backreflected for low- Z targets than for the high- Z ones (Z is the atomic number). Fluctuations around this rule are due to the statistical character of the MC method. Table I reveals that in gold and erbium, for hot temperatures higher than ~ 20 keV, more than 40% of the hot electrons energy is backreflected into the hot regions. An overall fit shows that the fraction of the backreflected energy, q_{backref} , can be reproduced by a power-law function to relatively good accuracy,

$$q_{\text{backref}} = (0.013 \pm 0.002) Z^{0.2 \pm 0.02} T_h \\ = (0.123 \pm 0.008) Z^{0.22 \pm 0.02} T_{15}^{0.085 \pm 0.005} \quad (20a)$$

(we recall that T_h is in eV). The maximum deviation of the MC results from this formula is 15%, but the *average* deviation is only $\sim 6\%$. Such accuracy is adequate for every practical purpose. The fraction of the absorbed energy is, of course, the complementary of Eq. (20a) to 1,

$$q_{\text{abs}} = 1 - q_{\text{backref}}. \quad (20b)$$

C. The energy deposition as a function of depth

Borrowing the ideas of SLA, we plotted the $J_0(y_0)$ [defined as the simulated energy deposition per atom, $\Delta E(x)$, divided by the coefficient on the right-hand side of Eq. (13)], as a function of the quantity y_0 (rather than x). Surprisingly, in the MC case, too, similarly to the SLA case, this function turned out to decrease exponentially to a high degree of accuracy, see Fig. 2. For all the cases in our study, we fitted the $J_0(y_0)$ function to an exponential one,

$$J_0(y_0) = A e^{-ay_0}, \quad (21)$$

where A and a are free parameters. The fit was always excellent. The values of A and a are given in Table I for all the cases in our study. In contrast to the SLA case, in the MC simulations the two coefficients have a dependence on Z and T_h . Both coefficients increase for higher Z and higher T_h . It is noteworthy, however, that this dependence is very slow, and a three-order of magnitude change in the laser intensity, generating a variation of $\times 10$ in the hot temperature, is re-

duced to a variation of less than 30% in either A or a . To account even for this small dependence, we have fitted these coefficients to a power-law function. The results are

$$A = (0.255 \pm 0.030) Z^{0.12 \pm 0.01} T_h^{0.22 \pm 0.01} \\ = (1.8 \pm 0.2) Z^{0.12 \pm 0.01} I_{15}^{0.073 \pm 0.03}, \quad (22)$$

$$a = (0.275 \pm 0.008) Z^{0.15 \pm 0.01} T_h^{0.19 \pm 0.01} \\ = (1.48 \pm 0.05) Z^{0.15 \pm 0.01} I_{15}^{0.063 \pm 0.002}. \quad (23)$$

The maximum deviation of the MC results from those of Eq. (22) is 20%, but the average deviation is less than 8%. Equation (23) fits the results of the simulations to an average accuracy better than 5%, and maximum deviation of 10%. Equations (21)–(23), in combination with Eqs. (13) and (10), provide tools of good accuracy for the calculation of the fast electron preheat in the cold material. These formulas are the central results of the present paper. Substitution of Eqs. (21)–(23) into Eq. (13) gives the following useful equation:

$$\Delta E(x) = (7.69 \times 10^{18} \text{ cm}^{-2}) \times q_{\text{abs}} Z^{0.12} \frac{\eta \tau_{L,\text{ps}}}{n_A} Q I_{15}^{0.74 - \alpha/3} \times \exp \left\{ -5.38 I_{15}^{-0.27} Z^{0.15} \right. \\ \left. \times \left[(1 + \alpha) \left(\frac{Q}{7 \times 10^7 \text{ eV/cm}} \right) x_{\mu\text{m}} \right]^{1/(1+\alpha)} \right\} \frac{\text{eV}}{\text{atom}}. \quad (24)$$

In Eq. (24) q_{abs} is the fraction of the absorbed energy, Eq. (20a). Using the parameters of aluminum, one gets for this material

$$\Delta E(x) = (10 \text{ } 100 \text{ eV}) \times q_{\text{abs}} \eta \tau_{L,\text{ps}} I_{15}^{0.4944} \\ \times \exp \left\{ -9.75 \times I_{15}^{-0.28} x_{\mu}^{0.5757} \right\} \frac{\text{eV}}{\text{atom}}. \quad (25)$$

This formula predicts that for $I_{15}=1$, the ratio $\Delta E(x)/\Delta E(x=0)$ drops to $1/e$ when $x=0.019 \mu\text{m}$, and to 0.01 at $x=0.27 \mu\text{m}$. The corresponding depths for gold ($\alpha=0.6593$, $B=7.47 \times 10^{10}$, $Q=21.79 \times 10^7 \text{ eV/cm}$) are much shorter, $x=0.0040 \mu\text{m}$ and $x=0.05 \mu\text{m}$, respectively.

The following points should be emphasized with respect to Eqs. (22)–(24): First, the relatively low powers of Z and T_h in these formulas reflect the low sensitivity of the two coefficients A and a on these variables. Second, the slope of the exponential function a is significantly larger than the slope in the SLA, as can be seen in Fig. 2. In fact, all the a coefficients in Table I for aluminum are much larger than the value $a=1.17$ obtained by the SLA. Similar results were obtained for all the other materials as well. This means that the MC simulations predict, as expected, that the fast electron energy is dumped into a thinner layer of atoms than

under the less realistic assumptions of the SLA. Finally, when only a part of the energy is absorbed, Eq. (16) is modified into the form,

$$A = q_{\text{abs}} a^{1+\alpha} / \Gamma(1+\alpha), \quad (26)$$

where q_{abs} is the fraction of the absorbed energy. We have found that this relationship is fulfilled to within 10–20%, and as already mentioned, this can be regarded as a measure of the deviation of $J_0(y_0)$ from an accurate exponential form.

D. The preheat temperature and pressure in the target

The energy transferred to the cold atoms by the suprathermal electrons is divided among the atom's ionization energy plus the kinetic energy of the released electrons plus the kinetic energy of the ion,

$$\Delta E(x) = \overline{\varepsilon(T)} + \frac{3}{2} \overline{Z(T)} T + \frac{3}{2} T \\ = \overline{\varepsilon(T)} + \frac{3}{2} [\overline{Z(T)} + 1] T. \quad (27)$$

In Eq. (27) $T=T(x)$ is the preheat temperature at depth x , $\overline{\varepsilon(T)} = \sum_{\zeta=1}^Z \varepsilon_{\zeta} N_{\zeta}(T) / n_A$ is the average energy invested into the ionization of the various charge species (ε_{ζ} is the energy required to ionize a neutral atom into a ζ -ply charged ion),

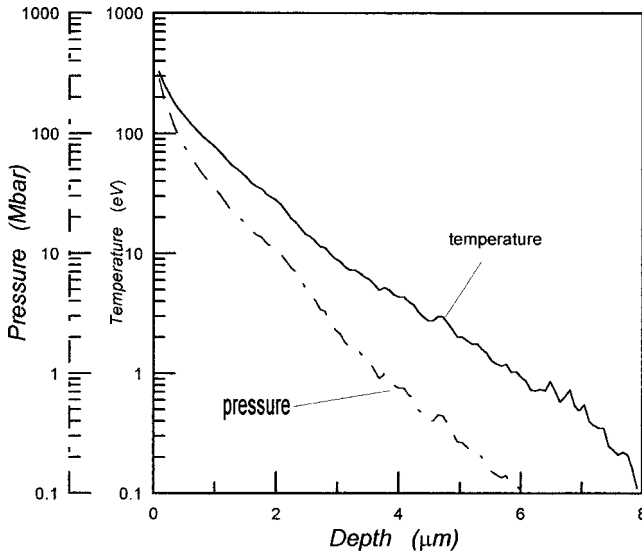


FIG. 3. The local temperature and pressure developing in a cold aluminum target hit by a $T_h = 7$ keV suprathermal electron beam, from a $I_L \lambda^2 = 10^{15}$ W $\mu\text{m}/\text{cm}^2$ laser irradiation.

$N_\zeta(T)$ is the density of ions having charge ζ , and $\overline{Z(T)} = \sum_{\zeta=1}^Z \zeta N_\zeta(T) / n_A$ is the average charge. Formula (27) is an equation from which one can solve the preheat temperature $T(x)$ in the cold material. When $T(x)$ is known, the preheat pressure $P(x)$, developed in the cold material, is calculated from

$$P(x) = n_e T(x) + n_A T(x) = \{\overline{Z[T(x)]} + 1\} n_A T(x). \quad (28)$$

The partial densities, $N_\zeta(T)$, as well as $\overline{\varepsilon(T)}$ and $\overline{Z(T)}$ were computed by means of a separate computer program which computes these quantities within the framework of the collisional-radiative model [16]. To exemplify the results of this paper we have solved Eqs. (27) and (28) for $T(x)$ and $P(x)$ in an aluminum plasma at laser-irradiation intensity of $I_L = 10^{15}$ W/cm², corresponding to a hot temperature $T_h = 7$ keV. The results are plotted in Fig. 3. Figure 3 indicates that relatively high temperatures develop on the layers near the critical surface. This region comes, however, rapidly to thermal balance with its hot vicinity through thermal electron conductivity.

In a plasma generated under these irradiation conditions, the shock wave that propagates into the cold substrate has a temperature of $T_{\text{shock}} = 4$ eV and pressure of $P_{\text{shock}} = 5.4$ Mbar [17]. The two pressures, P_{shock} and $P(x)$, are about equal at $x = 2.2$ μm , and the shock pressure exceeds the preheat pressure by factors of $\times 10$ and $\times 100$ at depths of $x = 4.1$ μm and $x \sim 7$ μm , respectively.

IV. SUMMARY

A. Validity conditions for the results

Obviously, the fast electron preheat is not an important effect below $I_L \lambda^2 < 10^{13}$ W $\mu\text{m}^2/\text{cm}^2$. This can be regarded as the low-intensity limit for the validity of our results. On

the other hand, above $I_L \lambda^2 > 10^{18}$ W $\mu\text{m}^2/\text{cm}^2$ relativistic effects become important, and these were not incorporated in our computer codes. Moreover, at such high intensities the forward running fast electrons generate a large charge separation, which drives a strong return current. This return current produces an additional heating that was not accounted for in our computations. Altogether, we can claim that the validity domain of our semiempirical formulas is

$$10^{13} \text{ W } \mu\text{m}^2/\text{cm}^2 < I_L \lambda^2 < 3 \times 10^{17} \text{ W } \mu\text{m}^2/\text{cm}^2. \quad (29)$$

This range has practical importance in a large range of laser-produced plasma experiments.

B. The accuracy of the results

The accuracy of our results is determined solely by the accuracy of the parameters of Eq. (2). All the other components have better accuracy, with 10–20% being a fair estimate for the overall inaccuracy of those parts of the formulas that are independent of Eq. (2). Such accuracy is sufficient for present day experimental purposes.

C. Comparison to Ref. [9]

We end this paper with a comparison to the results of Harrach and Kidder, Ref. [9]. Their paper is based on an unpublished NBS report by Spencer from 1959, which uses a moment method for the calculation of the electron transport, see their Ref. [3]. This report is not available anymore, and Ref. [9] does not provide adequate details about the underlying model. Judging, however, from some hints in [9], there seem to be similarities to our SLA. Their final result for the energy loss of a fast electron from the critical surface down to depth x (which is not exactly the quantity calculated in this paper), is an exponential function, $E_{\text{dep}}(x) \propto \exp\{-\beta \sqrt{x_0}\}$, where x_0 is proportional to the depth x , and β is a material-dependent quantity. This is rewritten as $E_{\text{dep}}(x) \propto \exp\{-\beta^* x^{0.5}\}$. Numerically, this is not too far from our Eq. (24), which gives $\Delta E(x) \propto \exp\{-\text{const} \times x^{1(1+\alpha)}\} = \exp\{-\text{const} \times x^{0.5757}\}$ for aluminum and $\Delta E(x) \propto \exp\{-\text{const} \times x^{0.6027}\}$ for gold, but nevertheless is not the same. We believe that our treatment has a better theoretical basis.

Regarding the other parts of their formulas, we find different behavior from ours as a function of the laser intensity, and their results dependence on the target material is listed only in a numerical form.

D. A short summary of the results of this paper

In this paper we describe a study of the preheat generated in the cold substrate by suprathermal electrons in laser-produced plasmas. Relatively simple semiempirical formulas having good accuracy are provided for the absorbed energy, the backreflected energy, Eq. (20), and the energy deposition per atom in the cold material, Eqs. (21)–(24). For illustration purposes we have also carried out a computation of the preheat temperature and pressure developing in an aluminum target by an $I_L \lambda^2 = 10^{15}$ W $\mu\text{m}^2/\text{cm}^2$ laser irradiation.

- [1] M. D. Rosen, D. W. Phillion, V. C. Rupert, W. C. Mead, W. L. Kruer, J. J. Thomson, H. N. Kornblum, V. W. Slivinsky, G. J. Caporaso, M. J. Boyle, and K. G. Tirsell, *Phys. Fluids* **22**, 2020 (1979).
- [2] Y. T. Lee and R. J. Trainor, LLNL Report No. UCID-18574-79-4, 1980.
- [3] J. C. Kieffer, H. Pepin, F. Martin, P. Church, T. W. Johnson, and R. Decoste, *Phys. Rev. Lett.* **44**, 1128 (1980).
- [4] W. C. Mead *et al.*, *Phys. Rev. Lett.* **47**, 1289 (1981).
- [5] N. M. Ceglio, D. T. Atwood, and J. T. Larsen, *Phys. Rev. A* **25**, 2351 (1982).
- [6] W. H. Goldstein and R. S. Walling, *Phys. Rev. A* **36**, 3482 (1987).
- [7] G. Malka *et al.*, *Phys. Rev. Lett.* **79**, 2053 (1997).
- [8] S. Bastiani *et al.*, *Phys. Rev. E* **56**, 7179 (1997).
- [9] R. J. Harrach and Ray E. Kidder, *Phys. Rev. A* **23**, 887 (1981).
- [10] K. G. Estabrook and W. L. Kruer, *Phys. Rev. Lett.* **40**, 42 (1978).
- [11] S. T. Perkins, D. E. Cullen, and S. M. Seltzer, UCRL-50400, 1991, Vol. 31.
- [12] A. F. Akkerman (private communication).
- [13] M. E. Riley *et al.*, *At. Data Nucl. Data Tables* **15**, 443 (1975); **28**, 379 (1983).
- [14] V. Cosslett and J. Thomas, *Brit. J. Appl. Phys.* **15**, 883 (1964); **16**, 779 (1965).
- [15] K. Riemer and H. Drechsler, *J. Phys. D* **10**, 805 (1977).
- [16] D. Salzmänn and A. D. Krumbein, *J. Appl. Phys.* **49**, 3229 (1978).
- [17] D. Salzmänn, S. Eliezer, A. D. Krumbein, and L. Gitter, *Phys. Rev. A* **28**, 1738 (1983).